

A Biologically Inspired Simultaneous Localization and Mapping System Based on LiDAR Sensor

Genghang Zhuang¹, Zhenshan Bing¹, Jiayi Zhao¹, Ning Li¹, Yuhong Huang¹, Kai Huang², and Alois Knoll¹

Abstract—Simultaneous localization and mapping (SLAM) is one of the essential techniques and functionalities used by robots to perform autonomous navigation tasks. Inspired by the rodent hippocampus, this paper presents a biologically inspired SLAM system based on a LiDAR sensor using a hippocampal model to build a cognitive map and estimate the robot pose in indoor environments. Based on the biologically inspired model, the SLAM system using point cloud data from a LiDAR sensor is capable of leveraging the self-motion cues from the LiDAR odometry and the local view cues from the LiDAR local view cells to build a cognitive map and estimate the robot pose. Experiment results show that the proposed SLAM system is highly applicable and sufficiently accurate for LiDAR-based SLAM tasks in both simulation and indoor environments.

I. INTRODUCTION

Simultaneous localization and mapping (SLAM), as one of the essential techniques and functionalities used by robots to perform autonomous navigation tasks [1], aims to build a map to construct a spatial representation of the unknown environment, and simultaneously locate the robot on the map being built. A large amount of research focuses on solving the SLAM problem with various types of sensors [2], [3], including monocular and stereo cameras, RGB-D cameras, and LiDAR sensors. Compared to camera sensors, LiDAR sensors are capable of obtaining more accurate distance and depth information by actively projecting laser beams, and are less subject to illumination changes in the environment. Hence, LiDAR sensors are widely used in autonomous driving and a considerable amount of research has been performed on using LiDAR sensors to resolve the SLAM problem [3]–[5], and other autonomous driving tasks including object detection [6], classification [7], and tracking [8].

In regard to mammals, research findings have shown that animals such as rodents have a different navigation system. Mammals are born with instinctive abilities and skills to perform navigation and cognition tasks. Successful discoveries have been made in investigating and understanding the spatial representation and navigation system of mammalian brains. Studies from neuroscience [9] have revealed that the hippocampus and entorhinal cortex play an important role in spatial navigation by coordinating several types of neurons for different functionalities, including place cells [10], [11], head direction cells [12], and grid cells [13], [14].

An increasing number of studies have been inspired by the neural mechanisms to solve the SLAM problem. *RatSLAM* in [15] utilized place cells and head direction cells to build a hippocampal model named pose cell network to integrate odometry motion data and landmarks from vision sensors

when mapping. In addition, a considerable number of related studies have been published for this navigational model, employing many types of sensors, including cameras [16]–[19], RGB-D sensors [20], and sonar sensors [21].

With the advantages of LiDAR sensors including high accuracy and stability, significant potential exists to further improve the overall performance of the biologically inspired SLAM system by using LiDAR sensors. However, to date, little literature has been published with regard to LiDAR-based biologically inspired SLAM approaches. The main challenge for LiDAR-based biologically inspired SLAM methods lies in the high computational complexity, due to the large scale of LiDAR point cloud. In addition, biologically inspired methods involving loop closure also require a reliable algorithm to detect loop closures in real-time.

In this paper, we present a biologically inspired SLAM system based on a LiDAR sensor to build cognitive maps for indoor environments, which more closely mimics the navigation mechanism of mammals. The system, employing a LiDAR sensor as the primary sensor, consists of three major modules, which include the LiDAR odometry, LiDAR local view cells, and the pose cell network. Based on the pose cell network, the SLAM system using point cloud data from a LiDAR sensor is capable of leveraging self-motion cues from the LiDAR odometry and local view cues from the LiDAR local view cells to build a cognitive map and estimate the robot pose. Specifically, the main contributions of this work are listed as follows:

- To fully leverage the advantages of the LiDAR sensor, a LiDAR odometry algorithm is implemented to generate pseudo-odometry data as the self-motion cues for the robot, to reduce the usage of physical odometric sensors such as IMU and wheel encoders that are prone to internal errors and noise.
- The local view cell model for the LiDAR sensor is implemented to provide local view cues to the pose cell network to perform pose calibration and loop closure detection. A two-stage local view matching approach is proposed to reduce the computational complexity of loop closure detection for LiDAR point cloud.
- The pose cell network model is adapted for the LiDAR sensor to implement the spacial location representation for the robot, and perform path integration and loop closure with the LiDAR self-motion cues and LiDAR local view cues. Experiment results show that the performance is highly applicable and sufficiently accurate in both simulation and indoor environments.

¹Department of Informatics, Technical University of Munich.

²School of Computer Science and Engineering, Sun Yat-sen University.

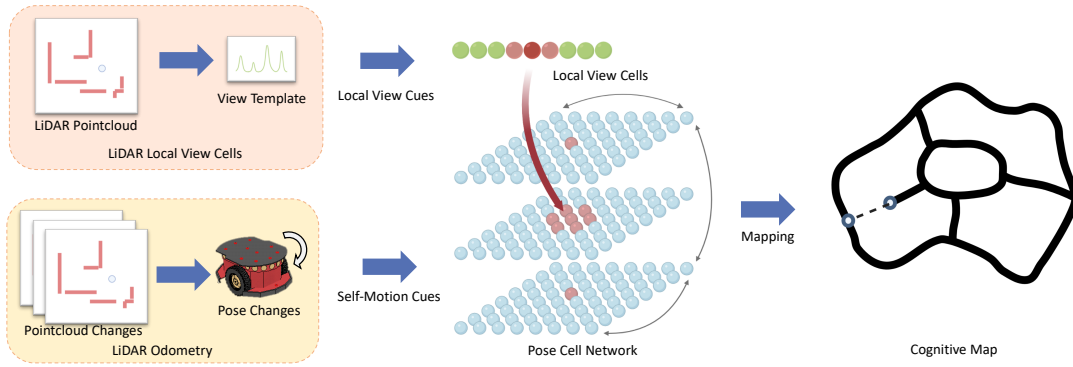


Fig. 1. System framework and major modules of the LiDAR-based biologically inspired SLAM system. The system is composed of the LiDAR odometry, LiDAR local view cells, and the pose cell network.

II. RELATED WORK

A. Conventional LiDAR SLAM

Error accumulation in point cloud matching and odometry drift is one of the main challenges of LiDAR-based SLAM. A number of studies have attempted to tackle this problem. Kohlbrecher et al. [4] proposed a scan-to-map matching algorithm with multi-resolution maps to reduce the matching errors. A LiDAR-based SLAM algorithm proposed by Grisetti et al. [22] utilized particle filters to reduce the odometry drift while mapping. However, these algorithms without loop closure calibration are still subject to cumulative sensor errors over long time mapping. Hess et al. [5] proposed the Cartographer SLAM system, which could perform loop closure detection for LiDAR SLAM to further improve the accuracy of mapping and localization. To detect loop closures, the system regularly runs the global pose optimization, in which the LiDAR scan is matched with all collected submaps to find the closest submap and update the pose estimate. It requires the loop closure detection to complete before the new scan being received.

B. Brain-Inspired Navigation

A number of studies were investigated to solve the SLAM problem with biologically inspired methods. Milford et al. proposed *RatSLAM* [15] to utilize the pose cell network to perform loop closure detection and solve the SLAM problem based on a camera sensor. Experimental results in [18], [19] also show the applicability of their proposed system in large-scale scenarios. Zhou et al. [17] employed the ORB features for the camera sensor to improve loop closure detection when mapping. Tian et al. [20] proposed an RGB-D sensor-based SLAM method with the pose network, and *BatSLAM* [21] combined the mapping module of *RatSLAM* and a sonar sensor to solve the SLAM tasks. However, in the related literature, it is rare that studies have focused on biologically inspired SLAM approaches using LiDAR sensors.

III. METHODOLOGY

The proposed biologically inspired SLAM system uses a LiDAR as the main sensor and data source. The architecture of the SLAM system is illustrated in Fig. 1. LiDAR odometry plays an important role in generating motion data for the

robot. The local view cells module provides local view cues that are processed and integrated based on the LiDAR observation. The pose cell network estimates the robot 3-DoF pose $\mathbf{p} = (x, y, \theta)^T$ by performing path integration and loop closure based on the self-motion data from LiDAR odometry and local view cues from the local view cell module.

A. LiDAR Odometry

The LiDAR odometry in the SLAM system provides odometric motion data for the pose cells to update the network state and perform path integration. Receiving consecutive point clouds from the LiDAR sensor, the aim of the LiDAR odometry is to estimate the pose change $\Delta \mathbf{p} = (\Delta x, \Delta y, \Delta \theta)$ during the time period of the robot movement.

The LiDAR sensor rotates in the horizontal plane and scans the surrounding objects with a fixed angle increment based on the angular resolution of the LiDAR sensor. A point cloud P from a complete scan can be defined as a sequence of endpoint distances as follows:

$$P = (d_i, i = 1, 2, \dots, N), \quad (1)$$

where d_i is the distance of the i -th scan endpoint, and N is the number of points in a complete scan, which is determined by the scanning angular resolution of the LiDAR sensor.

To estimate the pose change $\Delta \mathbf{p}$ with a given new input point cloud, the points are first transformed into the form of \mathbb{R}^2 Cartesian coordinate $\mathbf{e} = (x, y)^T$ as follows:

$$\mathbf{e}_i = \begin{pmatrix} d_i \cdot \cos \alpha_i \\ d_i \cdot \sin \alpha_i \end{pmatrix}, \quad (2)$$

where α_i is the corresponding scanning angle of the i -th endpoint.

In this work, local LiDAR mapping on an occupancy grid map is adopted to compute the pose change. A local occupancy grid map \mathbf{M} is employed to downsample the accumulation of LiDAR observations and reduce the effect of the sensor noise and dynamic obstacles [23]. The point cloud from LiDAR observation is matched against the local map to reduce the cumulative drift in scan-to-scan matching [4].

To estimate the pose change $\Delta \mathbf{p}$, a nonlinear optimization is constructed and performed to find the objective pose change $\Delta \mathbf{p}'$, where the current LiDAR point cloud can

best match the local map \mathbf{M} after being projected. The optimization objective is defined as follows:

$$\Delta \mathbf{p} = \arg \max_{\Delta \mathbf{p}'} \sum_i^N \mathbf{M}^* \left(\mathbf{R}_{\Delta \mathbf{p}'} \cdot (\mathbf{R}_{\mathbf{p}} \cdot \mathbf{e}_i + \mathbf{T}_{\mathbf{p}}) + \mathbf{T}_{\Delta \mathbf{p}'} \right), \quad (3)$$

where \mathbf{p} is the current pose of the robot, which is initialized as $\mathbf{p} = (0, 0, 0)^T$. \mathbf{M}^* is an upsampled local map of \mathbf{M} to provide a continuous occupancy function for the discrete grid map \mathbf{M} [4]. $\mathbf{R}_{\mathbf{p}}$ and $\mathbf{T}_{\mathbf{p}}$ are the corresponding rotation and translation transforms for a given pose $\mathbf{p} = (x, y, \theta)^T$:

$$\mathbf{R}_{\mathbf{p}} \cdot \mathbf{e} + \mathbf{T}_{\mathbf{p}} = \begin{pmatrix} \cos \theta & -\sin \theta \\ \sin \theta & \cos \theta \end{pmatrix} \cdot \mathbf{e} + \begin{pmatrix} x \\ y \end{pmatrix}. \quad (4)$$

The input point cloud is initially transformed to the local map with the current pose \mathbf{p} . The objective $\Delta \mathbf{p}'$ is optimized to yield the pose change estimate $\Delta \mathbf{p} = (\Delta x, \Delta y, \Delta \theta)$ as the output of LiDAR odometry, which is used to update the activity of pose cells and perform path integration.

B. LiDAR Local View Cells

The LiDAR local view cells module processes the LiDAR observations into view templates, which are feature information to represent the scenes. Local view templates are used to maintain the local views and provide the local view cue information to the pose cell network. The real-time LiDAR observation inputs will be compared with the previously learned local views to generate a pose calibration activity if a matched view is successfully found, or to learn a new local view if none is matched, by adding it into learned local views.

To balance the algorithm complexity and view matching accuracy, a two-stage local view matching approach is proposed in this work. In the first stage, coarse prematching is performed to boost the real-time performance and reduce the computational complexity. A coarse view feature for the LiDAR observation is proposed to roughly describe the point cloud by utilizing the aggregate of the scanning distances. The coarse view feature h is defined as follows:

$$h = \left\lfloor 10^{-d_s} \cdot \sum_i^N d_i \right\rfloor, \quad (5)$$

where d_s is a constant downscaling factor to specify the accuracy of the coarse matching. The coarse view feature h can be considered a hash value of the LiDAR observation, which is leveraged to reduce unnecessary matching processes in the second stage.

In the second refined matching stage, a LiDAR view template T is computed by downsampling the input point cloud P , which can be defined as a sequence:

$$T = \left(L\left(\frac{N}{M} \cdot i\right), i = 1, 2, \dots, M \right), \quad (6)$$

in which M is the parameterized size of the downsampled template, and $L(n)$ is a linear interpolation function for the point cloud P :

$$L(n) = d_{\lfloor n \rfloor} + (n - \lfloor n \rfloor) \cdot (d_{\lceil n \rceil} - d_{\lfloor n \rfloor}). \quad (7)$$

Algorithm 1 Naive Algorithm for Local View Matching

Input: Point cloud P_{in}

Output: Local view cells V

Initialization :

1: $found \leftarrow False$

2: $v_{in} \leftarrow \langle h_{in}, T_{in} \rangle$

3: $i \leftarrow 0$

Local View Matching

4: **for** $v_i = \langle h_i, T_i \rangle$ in learned views **do**

5: $V_i \leftarrow 0$

6: **if** $(h_i = h_{in})$ **then**

7: $s_i \leftarrow S(T_i, T_{in})$

8: **if** $(s_i < s_t)$ **then**

9: $found \leftarrow True$

10: $V_i \leftarrow 1 - s_i/s_t$

11: **end if**

12: **end if**

13: $i \leftarrow i + 1$

14: **end for**

15: **if not** $found$ **then**

16: Add v_{in} to learned views

17: Extend and update V

18: **end if**

19: **return** V

Hence, a LiDAR local view v is constructed as a tuple of the coarse view feature h and the view template T :

$$v = \langle h, T \rangle. \quad (8)$$

A new incoming local view will be compared with the learned local views and will be learned in the case no present local view succeeds to match.

In the local view matching process, the coarse view feature h is first estimated and compared to exclude dissimilar views. For the local views with the equal coarse view feature h , the corresponding view templates are second compared to estimate the template similarity $s = S(T_i, T)$, which is measured by computing the mean squared differences between the two view templates:

$$S(T_1, T_2) = \min_j \frac{1}{M} \sum_i^M (T_1(i+j) - T_2(i))^2, j \in [-\beta, \beta], \quad (9)$$

where β is the parameter of matching angular tolerance to allow a small deviation in the heading angle between the two view templates. The similarity s is used to determine whether the selected learned local view v_i is matched with the current local view v .

The local views are associated with the local view cells V , which is defined as a vector of cell activity levels. To maintain the matching levels over time for each local views, the activity of each cell will be updated as follows:

$$V_i = 1 - \frac{\min(s_t, S(T_i, T))}{s_t}, \quad (10)$$

where s_t is the matching threshold for similarity. The activity level of each cell is calculated based on the matching error between the local view $v = \langle h, T \rangle$ for the current LiDAR observation and the i -th learned local view $v_i = \langle h_i, T_i \rangle$, in which the error is clamped, inverted, and scaled to $[0, 1]$. In the event that no present local view is matched, the local view cell vector V will be extended to V_{i+1} to associate the new local view. The two-stage matching algorithm is formulated in Algorithm 1. Finally, the activity of local view cells V is output to the pose cell network to perform pose association for a new local view or loop closure for learned local views.

C. Pose Cell Network

In this work, we adopt the pose cell network inspired by *RatSLAM* to maintain the pose representation and integrate self-motion cues from LiDAR odometry and the local view cues from LiDAR local view cells, which is designed to reduce odometry drift and solve local view ambiguity in the process of mapping. Leveraging the pose cell network enables the proposed SLAM system to build a cognitive map by performing path integration based on self-motion cues. In addition, with the LiDAR view cues, the pose cell network can calibrate the estimated pose and the online cognitive map by performing loop closure to reduce the accumulated errors and drifts by LiDAR odometry.

The pose cell network is a 3D continuous attractor network (3D-CAN) [24], which can be represented as a 3D matrix of the activity: $\mathbf{PC}_{x',y',\theta'}$. The three dimensions of the pose cell network represent the three degrees of the 3-DoF pose $\mathbf{p} = (x, y, \theta)^T$, respectively, where $x', y', \theta' \in \mathbb{Z}$ are the discrete representation of $x, y, \theta \in \mathbb{R}$. Each pose cell unit in the pose cell network is connected with its neighbor units with excitatory and inhibitory connections, which wrap across the boundaries of the network in three dimensions to enable the pose cell network to represent an unbounded space with a limited number of pose cells [15].

The pose cell network enrolls local excitation and global inhibition activities, which are based on a three-dimensional Gaussian distribution, to self-update the pose cell network dynamics over time [19]. The stable state of the pose cell network, in which the activated cells are clustered, encodes the estimate of pose \mathbf{p} as the centroid of the activity packet [25].

Driven by the robot motion, the path integration updates the activity of the pose cells based on the self-motion cues from the LiDAR odometry detailed in SECTION III-A. The activity of each pose cell is shifted along with the translational and rotational movement based on the pose change $\Delta\mathbf{p} = (\Delta x, \Delta y, \Delta\theta)$. The activity update for each pose cell is defined as follows:

$$\Delta\mathbf{PC}_{x',y',\theta'} = \sum_{i=\delta_x}^{\delta_x+1} \sum_{j=\delta_y}^{\delta_y+1} \sum_{k=\delta_\theta}^{\delta_\theta+1} r_{ijk} \cdot \mathbf{PC}_{(x'+i),(y'+j),(\theta'+k)} \quad (11)$$

$$\delta_x = \lfloor k_x \Delta x \rfloor, \delta_y = \lfloor k_y \Delta y \rfloor, \delta_\theta = \lfloor k_\theta \Delta \theta \rfloor,$$

where r_{ijk} is a residue based on the fractional part of the pose changes spread over the $2 \times 2 \times 2$ cube to reduce

the precision loss by quantization [15], k_x, k_y, k_θ are the constant scaling factors for the three dimensions.

Given the LiDAR local view cues from the local view cells, a calibrating activity is injected into the pose cell network to perform further loop closure and re-localization. The activity of each pose cell is updated based on the activity of local view cells V , as defined as follows:

$$\Delta\mathbf{PC}_{x',y',\theta'} = k_V \cdot \sum_i \mathbf{A}_{i,x',y',\theta'} \cdot V_i, \quad (12)$$

where k_V is the constant calibration rate, and $\mathbf{A}_{i,x',y',\theta'}$ is an adjacency matrix for the connections from the local view cells to the pose cells. When a new local view V_i is learned, an excitatory link from V_i to the current state of the pose cell network (x', y', θ') is established, where $\mathbf{A}_{i,x',y',\theta'}$ is accordingly set to 1. To solve the local view ambiguity, only updates by consecutive local views over the threshold can shift the main activity packet of the pose cells.

In the mapping process, the information from the LiDAR odometry, LiDAR local view cells, and the pose cells are combined and accumulated to estimate the robot pose $\mathbf{p} = (x, y, \theta)^T$ in the \mathbb{R}^3 space, and build a cognitive map as a topological graph of robot movement experiences. A node in the cognitive map is an experience node defined as a tuple of the states of the pose cells \mathbf{PC} , the local view cells V , and the pose estimate \mathbf{p} :

$$e_i = \langle \mathbf{PC}^i, V^i, \mathbf{p}^i \rangle. \quad (13)$$

After a period of robot movement, when a new local view is learned, a new experience node e^j , separate from the previous node e^i , is created based on the pose change $\Delta\mathbf{p}^{ij}$. Then the two experience nodes are connected with a directed edge from e^i to e^j based on the pose transition l_{ij} , which is defined as follows:

$$e_j = \langle \mathbf{PC}^j, V^j, \mathbf{p}^i + \Delta\mathbf{p}^{ij} \rangle, \quad (14)$$

$$l_{ij} = \langle \Delta\mathbf{p}^{ij}, \Delta t^{ij} \rangle.$$

When a learned local view is observed and loop closure is detected, a new transition between two existing experience nodes is established, which results in a new cycle in the cognitive map. The pose transition $\Delta\mathbf{p}$ of each node and edge is accordingly updated as follows to distribute the accumulated odometry error over the trails, and update the pose estimate $\mathbf{p} = (x, y, \theta)^T$ of the robot.

$$\Delta\mathbf{p}^i = a \left[\sum_{j=1}^{N_f} (\mathbf{p}^j - \mathbf{p}^i - \Delta\mathbf{p}^{ij}) + \sum_{k=1}^{N_t} (\mathbf{p}^k - \mathbf{p}^i - \Delta\mathbf{p}^{ki}) \right], \quad (15)$$

where a is a constant correction factor set to 0.5, N_f and N_t are the number of the outgoing and incoming edges of e_i . Hence, the cognitive map and the pose estimate \mathbf{p} are obtained and updated online as the output of the proposed LiDAR-based biologically inspired SLAM system.

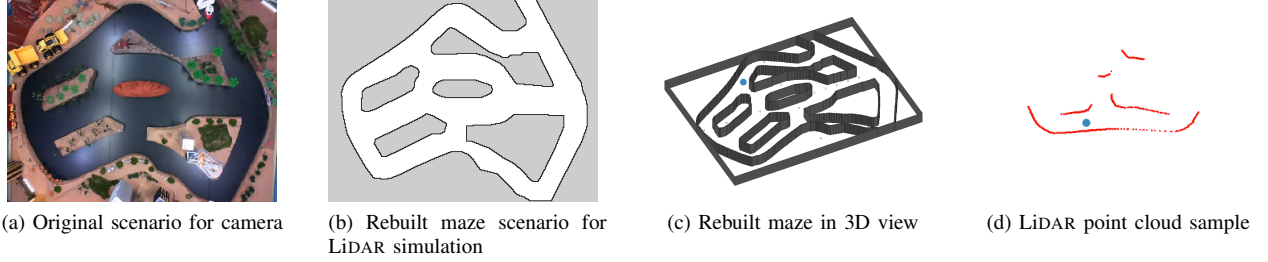


Fig. 2. Overview of the maze simulation scenario.

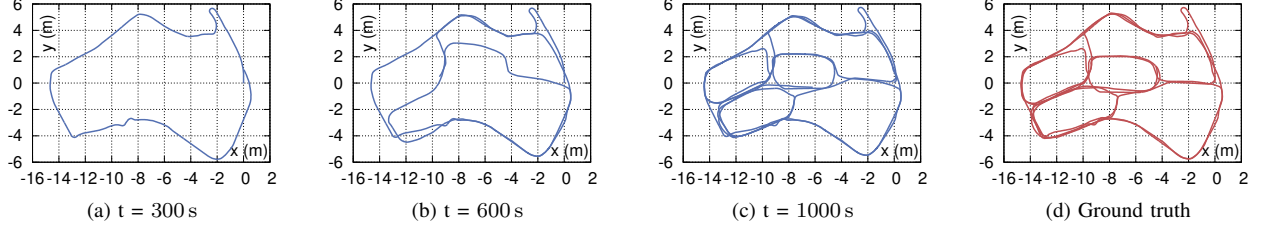


Fig. 3. Mapping progress in the maze simulation scenario.

IV. EXPERIMENTS

In this section, we present the experimental results for the proposed approach. To evaluate the LiDAR-based biologically inspired SLAM system, experiments are conducted in both simulation and real indoor scenarios to investigate the mapping and localization performance. The proposed SLAM system is implemented and tested on the *Robot Operating System* (ROS) [26]. We first report the experimental results of a simulation experiment to evaluate the mapping performance as well as the localization accuracy. Second, a mapping experiment in an indoor environment based on a ground robot is detailed. The results of the indoor experiment are illustrated and analyzed to demonstrate the applicability and accuracy of the proposed SLAM system in the real world.

A. Simulation Experiment

In the simulation experiments, a maze scenario is ported from the *iRat 2011 Australia* dataset [25], which is originally designed for the visual *RatSLAM*. Since the original dataset does not include LiDAR sensor data, it is not feasible to carry out the LiDAR SLAM experiments using the dataset. Therefore, we rebuild the maze scenario in the simulator to make it suitable for LiDAR-based simulations.

Fig. 2 gives an overview of the maze scenario. Utilizing the *Stage* simulator in the ROS framework, the point cloud data for a robot spawned in the maze scenario are obtained from a configurable virtual LiDAR in the simulator. At the same time, the ground truth information of the poses and movements of robots are also collected for evaluation purposes, but the odometry data is not involved in the SLAM process. Only the LiDAR point cloud data are used in the proposed method.

In the simulation experiment, the robot is controlled manually to navigate the maze for 1,200 seconds to evaluate the mapping performance with loop closure during long-term mapping. Fig. 3 illustrates the progressive cognitive maps

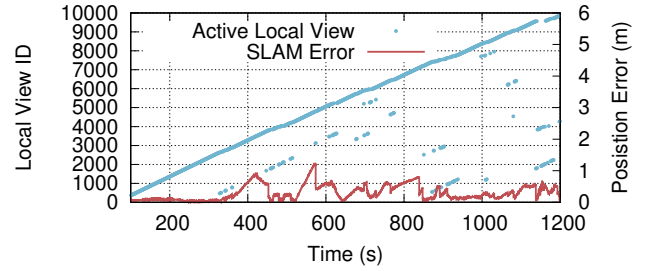


Fig. 4. Active local view cell over time in simulation.

built by the SLAM system in the simulation experiment and the ground truth path provided by the ROS Stage simulator. As shown in the mapping progress over time, the error in the cognitive map is gradually reduced over time. The mapping result of high similarity to the ground truth path demonstrates that SLAM performance is sufficiently accurate.

Fig. 4 reveals the activity of the local view cells, which further reflects the loop closure detection and calibration of the cognitive map and the robot pose estimate. The number of local view cells increases as the robot keeps moving to unexplored scenes, which are learned as the new local views. This is consistent with Fig. 4, in which the increase of the local view ID composes the main part of the scatter plot. The figure also reveals the loop closure detection during the mapping progress. The dramatic decrease in the active local view ID indicates that a number of previously learned local views are matched with the current LiDAR observation. Combining Fig. 3 and Fig. 4, it is obvious that during the mapping process, at around 330 s the proposed SLAM started to detect the previously learned views and performed loop closure calibration to reduce the accumulated error in the map, which demonstrates the ability of the local view cells to detect loop closure in the mapping process.

In Fig. 4 we also report the localization error during the mapping process in the simulation experiment. The translational error computed based on the ground truth data ranges from 0.0027 m to 1.2222 m, with a mean value of

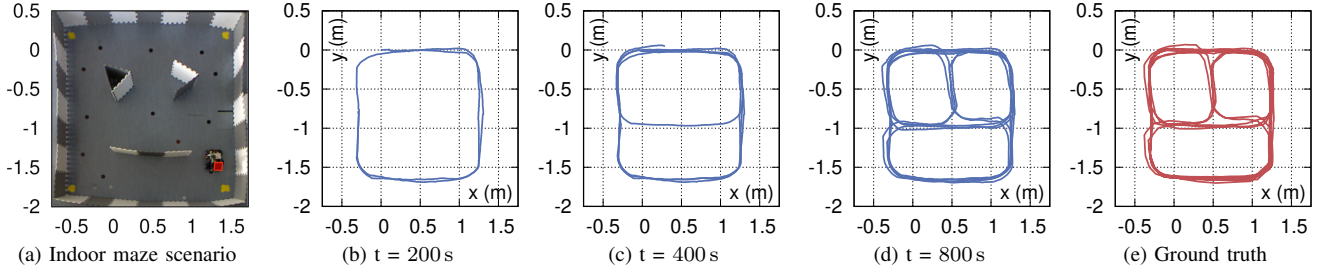


Fig. 5. Mapping progress in the real indoor maze environment.

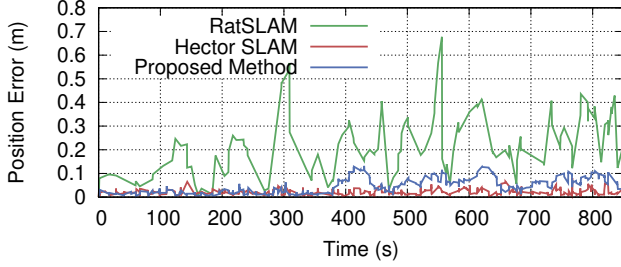


Fig. 6. Translational errors over time in the maze mapping process.

0.2985 m, for the 1,200 seconds of the mapping process in the $16.8\text{ m} \times 12.6\text{ m}$ space. As shown in the graph, the error remains at a low level for the whole mapping process. For several periods of time around 380 s, 470 s, and 660 s, the position error started to accumulate but was soon corrected after a period of time. The transition of the accumulated error shows the process of loop closure detection and demonstrates the high performance of the proposed SLAM system for both mapping and localization.

B. Indoor Experiment

To further evaluate the performance of the proposed SLAM system, experiments were conducted in a real indoor scenario, based on a ground robot platform. The ground robot is driven by four differential wheels which are controlled by an embedded *Raspberry Pi 3* single-board computer. A 2D *Hokuyo UTM-30LX-EW* LiDAR sensor is installed on the robot to obtain LiDAR point cloud for mapping experiments.

To specifically evaluate the mapping accuracy in the experiments, as shown in Fig. 5a, we built a maze experimental environment with an external localization and tracking system based on a bird view camera. In the indoor maze experiment, the robot was controlled to continuously navigate the maze for a specified period of time, while the bird view camera kept tracking the movements of the robot in real time to provide the ground truth for localization evaluation in parallel.

The progress of the mapping experiment for 900 s in the maze settings is illustrated in Fig. 5 from Fig. 5b to Fig. 5d, in which each cognitive map was taken at the annotated intervals during the mapping process. To further quantify the localization and mapping performance, in the indoor experiments, we additionally introduce two related SLAM algorithms for comparison purposes. To date, since it is rare that studies have focused on LiDAR-based biologically inspired SLAM algorithms, we evaluated *RatSLAM* [25],

which is based on a camera sensor and is one of the most commonly used biologically-inspired SLAM system. In addition, the experiments also include a conventional LiDAR-based SLAM system named *Hector SLAM* [4], which is one of the state-of-art indoor SLAM methods [3]. We mainly evaluated the SLAM accuracy for the involved SLAM methods in the same experimental settings. In the experiments, translational errors are computed based on the estimated poses given by the SLAM algorithms and the real-time ground-truth poses given by the bird view camera. Fig. 6 shows the position error curves of the proposed method, *RatSLAM*, and *Hector SLAM*, during the mapping process of the indoor maze environment. As shown in the figure, the error curve of *RatSLAM* fluctuated more dramatically than that of the proposed biologically-inspired method and *Hector SLAM*. The position error of the proposed SLAM system is much stabler and lower than *RatSLAM* and is close to the state-of-art conventional SLAM method *Hector SLAM*. In the second half of the mapping process, the error of the proposed method started to accumulate at around 400 s and 600 s but was corrected soon and remained low. The Root Mean Square Error (RMSE) of the proposed method for the estimated poses in the indoor experiments is 5.35 cm. In comparison, the RMSE of *RatSLAM* is 25.4 cm and the value of *Hector SLAM* is 2.42 cm. The results demonstrate that the accuracy of the proposed LiDAR-based biologically-inspired SLAM method outperforms the vision-based biologically-inspired *RatSLAM* and the performance is close to that of the state-of-art conventional LiDAR SLAM method *Hector SLAM*.

V. CONCLUSION

In this paper, we present a novel biologically-inspired SLAM system that combines and leverages the LiDAR sensor and the pose cell network to perform cognitive mapping and localization for indoor environments. With the self-motion cues and the local view cues from the LiDAR odometry and LiDAR local view cells, the proposed SLAM system performs path integration and loop closure in the pose cell network to maintain and calibrate the robot pose estimates and build a cognitive map, which more closely mimics the navigation mechanism of mammals. Experimental results show that the proposed SLAM system is both applicable and sufficiently accurate in both the simulation scenario and the indoor environments, and is competitive to the state-of-art LiDAR-based SLAM method.

REFERENCES

- [1] S. Thrun, "Probabilistic robotics," *Communications of the ACM*, vol. 45, no. 3, pp. 52–57, 2002.
- [2] T. Taketomi, H. Uchiyama, and S. Ikeda, "Visual slam algorithms: a survey from 2010 to 2016," *IPSI Transactions on Computer Vision and Applications*, vol. 9, no. 1, p. 16, 2017.
- [3] J. M. Santos, D. Portugal, and R. P. Rocha, "An evaluation of 2d slam techniques available in robot operating system," in *2013 IEEE International Symposium on Safety, Security, and Rescue Robotics (SSRR)*. IEEE, 2013, pp. 1–6.
- [4] S. Kohlbrecher, O. Von Stryk, J. Meyer, and U. Klingauf, "A flexible and scalable slam system with full 3d motion estimation," in *2011 IEEE international symposium on safety, security, and rescue robotics*. IEEE, 2011, pp. 155–160.
- [5] W. Hess, D. Kohler, H. Rapp, and D. Andor, "Real-time loop closure in 2d lidar slam," in *2016 IEEE International Conference on Robotics and Automation (ICRA)*. IEEE, 2016, pp. 1271–1278.
- [6] B. Yang, W. Luo, and R. Urtasun, "Pixor: Real-time 3d object detection from point clouds," in *Proceedings of the IEEE conference on Computer Vision and Pattern Recognition*, 2018, pp. 7652–7660.
- [7] C. R. Qi, H. Su, K. Mo, and L. J. Guibas, "Pointnet: Deep learning on point sets for 3d classification and segmentation," in *Proceedings of the IEEE conference on computer vision and pattern recognition*, 2017, pp. 652–660.
- [8] A. Asvadi, P. Girão, P. Peixoto, and U. Nunes, "3d object tracking using rgb and lidar data," in *2016 IEEE 19th International Conference on Intelligent Transportation Systems (ITSC)*. IEEE, 2016, pp. 1255–1260.
- [9] E. I. Moser, E. Kropff, and M.-B. Moser, "Place cells, grid cells, and the brain's spatial representation system," *Annu. Rev. Neurosci.*, vol. 31, pp. 69–89, 2008.
- [10] J. O'Keefe and J. Dostrovsky, "The hippocampus as a spatial map: Preliminary evidence from unit activity in the freely-moving rat," *Brain research*, 1971.
- [11] J. O'Keefe, "Place units in the hippocampus of the freely moving rat," *Experimental neurology*, vol. 51, no. 1, pp. 78–109, 1976.
- [12] J. S. Taube, R. U. Muller, and J. B. Ranck, "Head-direction cells recorded from the postsubiculum in freely moving rats. i. description and quantitative analysis," *Journal of Neuroscience*, vol. 10, no. 2, pp. 420–435, 1990.
- [13] T. Hafting, M. Fyhn, S. Molden, M.-B. Moser, and E. I. Moser, "Microstructure of a spatial map in the entorhinal cortex," *Nature*, vol. 436, no. 7052, pp. 801–806, 2005.
- [14] M. E. Hasselmo, "Grid cell mechanisms and function: contributions of entorhinal persistent spiking and phase resetting," *Hippocampus*, vol. 18, no. 12, pp. 1213–1229, 2008.
- [15] M. J. Milford, G. F. Wyeth, and D. Prasser, "Ratslam: a hippocampal model for simultaneous localization and mapping," in *IEEE International Conference on Robotics and Automation, 2004. Proceedings. ICRA'04. 2004*, vol. 1. IEEE, 2004, pp. 403–408.
- [16] M. J. Milford and A. Jacobson, "Brain-inspired sensor fusion for navigating robots," in *2013 IEEE International Conference on Robotics and Automation*. IEEE, 2013, pp. 2906–2913.
- [17] S.-C. Zhou, R. Yan, J.-X. Li, Y.-K. Chen, and H. Tang, "A brain-inspired slam system based on orb features," *International Journal of Automation and Computing*, vol. 14, no. 5, pp. 564–575, 2017.
- [18] F. Yu, J. Shang, Y. Hu, and M. Milford, "Neuroslam: a brain-inspired slam system for 3d environments," *Biological Cybernetics*, vol. 113, no. 5-6, pp. 515–545, 2019.
- [19] M. J. Milford and G. F. Wyeth, "Mapping a suburb with a single camera using a biologically inspired slam system," *IEEE Transactions on Robotics*, vol. 24, no. 5, pp. 1038–1053, 2008.
- [20] B. Tian, V. A. Shim, M. Yuan, C. Srinivasan, H. Tang, and H. Li, "Rgb-d based cognitive map building and navigation," in *2013 IEEE/RSJ International Conference on Intelligent Robots and Systems*. IEEE, 2013, pp. 1562–1567.
- [21] J. Steckel and H. Peremans, "Batslam: Simultaneous localization and mapping using biomimetic sonar," *PloS one*, vol. 8, no. 1, p. e54076, 2013.
- [22] G. Grisetti, C. Stachniss, and W. Burgard, "Improved techniques for grid mapping with rao-blackwellized particle filters," *IEEE transactions on Robotics*, vol. 23, no. 1, pp. 34–46, 2007.
- [23] A. Elfes, "Using occupancy grids for mobile robot perception and navigation," *Computer*, vol. 22, no. 6, pp. 46–57, 1989.
- [24] A. Samsonovich and B. L. McNaughton, "Path integration and cognitive mapping in a continuous attractor neural network model," *Journal of Neuroscience*, vol. 17, no. 15, pp. 5900–5920, 1997.
- [25] D. Ball, S. Heath, J. Wiles, G. Wyeth, P. Corke, and M. Milford, "Openratslam: an open source brain-based slam system," *Autonomous Robots*, vol. 34, no. 3, pp. 149–176, 2013.
- [26] M. Quigley, K. Conley, B. Gerkey, J. Faust, T. Foote, J. Leibs, R. Wheeler, and A. Y. Ng, "Ros: an open-source robot operating system," in *ICRA workshop on open source software*, vol. 3, no. 3.2. Kobe, 2009, p. 5.